ADVANCED OPTICAL MATERIALS
www.advopticalmat.de

Electroluminescent Guest@MOF Nanoparticles for Thin Film Optoelectronics and Solid-State Lighting

*Mario Gutiérrez, Cristina Martín, Mark Van der Auweraer, Johan Hofkens, and Jin-Chong Tan**

Light-emitting diodes (LEDs) are an efficient source of lighting, with many commercial applications like general illumination, camera flashes, phone or laptop displays, and TV screens. However, they present certain limitations, including low-quality color rendition, and the use of expensive/toxic rare-earth elements. There is therefore an urgent need for the development of improved luminescent materials free of rare earths. Luminescent metal–organic framework (LMOF) materials are promising candidates for photonics devices. Most MOF-LEDs reported are of the down-converter type, where UV or blue LED are coated with LMOFs, however there is limited progress in the development of LED using LMOFs as the electroluminescent layer. Herein, it is reported a novel Guest@MOF composite synthesized by encapsulating a semiconducting Gaq3 metal complex [gallium(III) tris(8-hydroxyquinolinato)], into the ZIF-8 pore [Zn (2-methylimidazolate)$_2$], yielding a green-yellowish luminescent material exhibiting a relatively high quantum yield of 15% upon photoexcitation. Subsequently, a down-converter LED comprising 405-nm violet LED coated with Gaq3@ZIF-8, yielding a white MOF-LED is shown. Then the use of Gaq3@ZIF-8 as an electroluminescent layer in a hybrid-LED, achieving an orange-yellowish light emitting device is demonstrated. This work reveals the potential of LMOFs for next-generation LED technology, by exploiting the Guest@MOF concept to enable electroluminescent applications.

1. Introduction

One of the biggest challenges that the scientific community faces today is the development of new practical and cost-effective solutions to ensure sustainable global growth, addressing the issues of clean energy generation and energy conversion. Therefore, current efforts are focused on finding new sustainable lighting sources to meet the growing energy demand through engineering of smarter and more efficient devices. Light-emitting diodes (LEDs) are one of the most efficient lighting devices available today, presenting many advantages over traditional lighting such as incandescent or halogen bulbs. For instance, LEDs emit light in a more directed way, reducing the use of diffusers and reflectors, significantly, the heat released is 90% lower than incandescent bulbs, the life of LED is 3–25 times longer, and most importantly, the energy saving by a LED compared to incandescent and halogens bulbs can be as high as ≈80%.[1]

For the aforementioned reasons, white LEDs (WLEDs) have become one of the most commonly employed sources of light for illumination purposes. There exist two different approaches to fabricate WLEDs: i) RGB systems:[2] where the primary red, green and blue color emitters are combined in a controlled proportion to emit white light, and ii) Down-converter WLEDs: where typically a GaN or InGaN blue LED chip is coated with a yellow phosphor like Ce^{3+}:YAG or its derivatives, in which the combination of blue and yellow emitters produces white light.[3,4] Although these WLEDs have already presented important benefits over the traditional lighting sources, there are still challenges because of their limited efficiency (RGB devices), and/or unsatisfactory color rendering index (down-converter WLEDs), or most notably these devices require the use of expensive and toxic rare-earth elements.[4] The shortage of rare earths and their limited geological distribution have further elevated their prices, thus prompting the scientific community to develop alternative materials able to substitute rare-earth coated WLEDs to permit fabrication of next-generation lighting devices. Some of the already proposed materials include, but not limited to nanoparticles, quantum dots (QDs), organic molecules and polymers, but in most of those cases their practical use is reduced since their emission is strongly quenched in the solid state.[5–8]

Dr. M. Gutiérrez, Prof. J.-C. Tan
Multifunctional Materials & Composites (MMC) Laboratory
Department of Engineering Science
University of Oxford
Parks Road, Oxford OX1 3PJ, UK
E-mail: jin-chong.tan@eng.ox.ac.uk
Dr. C. Martín
Departamento de Química Física. Facultad de Farmacia de Albacete
UCLM
Albacete 02071, Spain
Dr. C. Martín, Prof. M. Van der Auweraer, Prof. J. Hofkens
Molecular Imaging and Photonics
Department of Chemistry
Katholieke Universiteit Leuven
Celestijnenlaan, 200F, Leuven 3001, Belgium
The ORCID identification number(s) for the author(s) of this article can be found under https://doi.org/10.1002/adom.202000670.

DOI: 10.1002/adom.202000670

The encapsulation of silver clusters (emissive species) inside the zeolites pores (host) have recently been proposed as a promising alternative for lighting applications.[9,10] They were reported to exhibit excellent optoelectronic properties, high thermal and environmental (oxygen and water) stability, and low toxicity.[11,12] Several studies have demonstrated their application as WLEDs,[13,14] however, the difficulties to tune the functional luminescent silver zeolites at will due to the limitations of the size and topology of the zeolite pore is forcing the scientific community to find alternatives for this aim. Among all the possibilities, highly tuneable emissive nanomaterials known as luminescent metal–organic frameworks (LMOFs) have emerged as one of the most promising candidates for the fabrication of next-generation of LED devices (MOF-LED). The combination of metal clusters interlinked by organic ligands jointly with their chemical flexibility (exchangeable metal clusters/organic linkers and post-synthetic functionalization) and their accessible nanoscale cavities (where functional guests may be confined)[15] have transformed MOFs into promising candidates to be implemented in a wide range of photonic applications,[16,17] including the LEDs.[18] Most of the MOF-LEDs reported up till now are down-converter type systems, where near-ultraviolet (NUV) or blue LEDs are coated with different LMOFs in order to get a final WLED device. A number of LMOFs and related Guest@MOF composites have already been demonstrated for this type of WLED development, here are a few examples found in literature: $[Zn_6(btc)_4(tppe)_2(DMA)_2]$,[19] LMOF-231,[20] MOF-253-Eu1-TTA,[21] carbon dots/Zr-MOF,[22] or $Ir(ppy)_2(bpy)$@Cd-H_6TATPT.[23] Although there is an increasing number of down-converter MOF-LEDs,[24,25] to the best of our knowledge there are just a few examples in the literature in which electroluminescent MOFs are integrated as the electroluminescent layers of the MOF-LEDs. These are reduced to $[ZnNa_2(L)_2(DEF)_2]\cdot DEF$ (NNU-27),[26] $Sr(ntca)(H_2O)_2\cdot H_2O$,[27] and Zr-NDC MOF and derivative guest@Zr-NDC composites,[28] which exhibit orange-red and white light emissions, respectively.

In this work, by leveraging our recently developed high-concentration reaction (HCR) synthetic approach,[29,30] we have accomplished a previously unreported light-emitting Guest@MOF composite system, termed Gaq3@ZIF-8, where the luminescent guest, Gaq3 [gallium(III) tris(8-hydroxyquinolinato)], is confined within the nanoscale pores of the ZIF-8 [Zn(2-methylimidazolate)$_2$] nanocrystals. While the Gaq3 dye is a very well-known semiconducting metal complex that has been used in the fabrication of hybrid/organic LEDs (OLEDs),[31–33] to date it has not been employed in the Guest@MOF context. Significantly, we found that the incorporation of Gaq3 (guest) into ZIF-8 (host) enhances its long-term stability because of the guest–host shielding effect. Indeed, we have demonstrated that this Gaq3@ZIF-8 nanomaterial is stable at least for 8 months with no changes either to its crystalline structure, or to its photoluminescence properties. The Gaq3@ZIF-8 composite exhibits a green-yellowish luminescence similar to Ce^{3+}:YAG phosphor or Alq3 complex,[34,35] with a relatively high quantum yield (≈15%) in the solid-state form. Encouraged by these results, we have fabricated two types of proof-of-concept LED devices: a) down-converter MOF-WLED, where a 405 nm LED was coated with Gaq3@ZIF-8, and b) a new MOF-LED in which Gaq3@ZIF-8 functions as the electroluminescent layer. Our results revealed the exciting potential of LMOFs for their implementation in LED technologies, paving the way to the development of new LMOFs with promising photophysical and electroluminescent properties to fill a gap in the almost unexplored field of multilayer electroluminescent MOF-LEDs.

2. Results and Discussion

2.1. Luminescent Guest@MOF Nanoparticles

We employ a rapid one-pot synthesis method to yield (Guest@MOF) Gaq3@ZIF-8 LMOFs using different amounts of Gaq3 (0.05, 0.5, and 2 mmol), the full details are described in the Experimental Section. Given the spherical pore of the ZIF-8 host (pore volume ≈1750 Å^3, estimated from Discovery Studio software)[36] it is feasible that the Gaq3 isodiametric metal complexes (guest volume ≈440 Å^3) are confined within the pores of ZIF-8 as illustrated in **Figure 1**A. In fact, after the synthesis of the Gaq3@ZIF-8 LMOFs, a thorough washing of the materials had to be done to remove all the excess Gaq3 metal complexes deposited on the surface of the MOF (see Figure S1 in the Supporting Information). The Gaq3@ZIF-8 LMOFs obtained after drying of solvent are in the form of pale-yellowish monoliths, which can be as large as 1.5 cm and exhibit an intense green-yellowish emission under a 365 nm UV irradiation (Figure 1B). Those monoliths were then ground into fine powders using a mortar and a pestle. The crystalline structure, morphology and chemical properties of the fine powders of Gaq3@ZIF-8 were characterized by means of powder X-ray diffraction (PXRD), atomic force microscopy (AFM), and Fourier-transform infrared (FTIR) techniques.

Figure 1D shows that the PXRD patterns of the different Gaq3@ZIF-8 composites (0.05, 0.5, and 2 mmol) are very similar to the pristine phase of ZIF-8, and resembling also the simulated pattern of ZIF-8. However, salient information can be extracted from the PXRD data. First, the high similitude between the PXRD patterns of ZIF-8 and the different Gaq3@ZIF-8 points out that there are no important structural changes in the ZIF-8 host upon encapsulation of the Gaq3 guests. Second, the broadening observed in all the Bragg peaks of Gaq3@ZIF-8 and pristine ZIF-8 (compared to the ZIF-8 simulated pattern) suggests the smaller size of our resulting MOF materials.[37] This is indeed in good agreement with the AFM topography of Gaq3@ZIF-8 (0.5 mmol), showing a nanosized crystal with a width of 150–200 nm and a height of 20–40 nm (Figure 1C), thus its nominal aspect ratio (width/height) is about 5:1. Moreover, the lack of peaks in the PXRD pattern associated with crystalline phases of Gaq3 is not surprising because of two main reasons: i) to detect Bragg diffraction peaks, the Gaq3 complexes should show a long-range periodic orientation, however due to the low concentration of guests they are likely randomly distributed within the ZIF-8 host, and ii) the weight % of Gaq3 in comparison to ZIF-8 is relatively low, and it is well-known that PXRD is not a very sensitive technique (detection limit is usually of the order of 5–10%).[37] On the contrary, the FTIR spectrum of Gaq3@ZIF-8 presents multiple bands which are a combination of the ones observed in the Gaq3 and the ZIF-8 spectra (Figure 1E). For example, the FTIR spectrum of Gaq3@ZIF-8 shows absorption bands above 1000 cm^{-1}

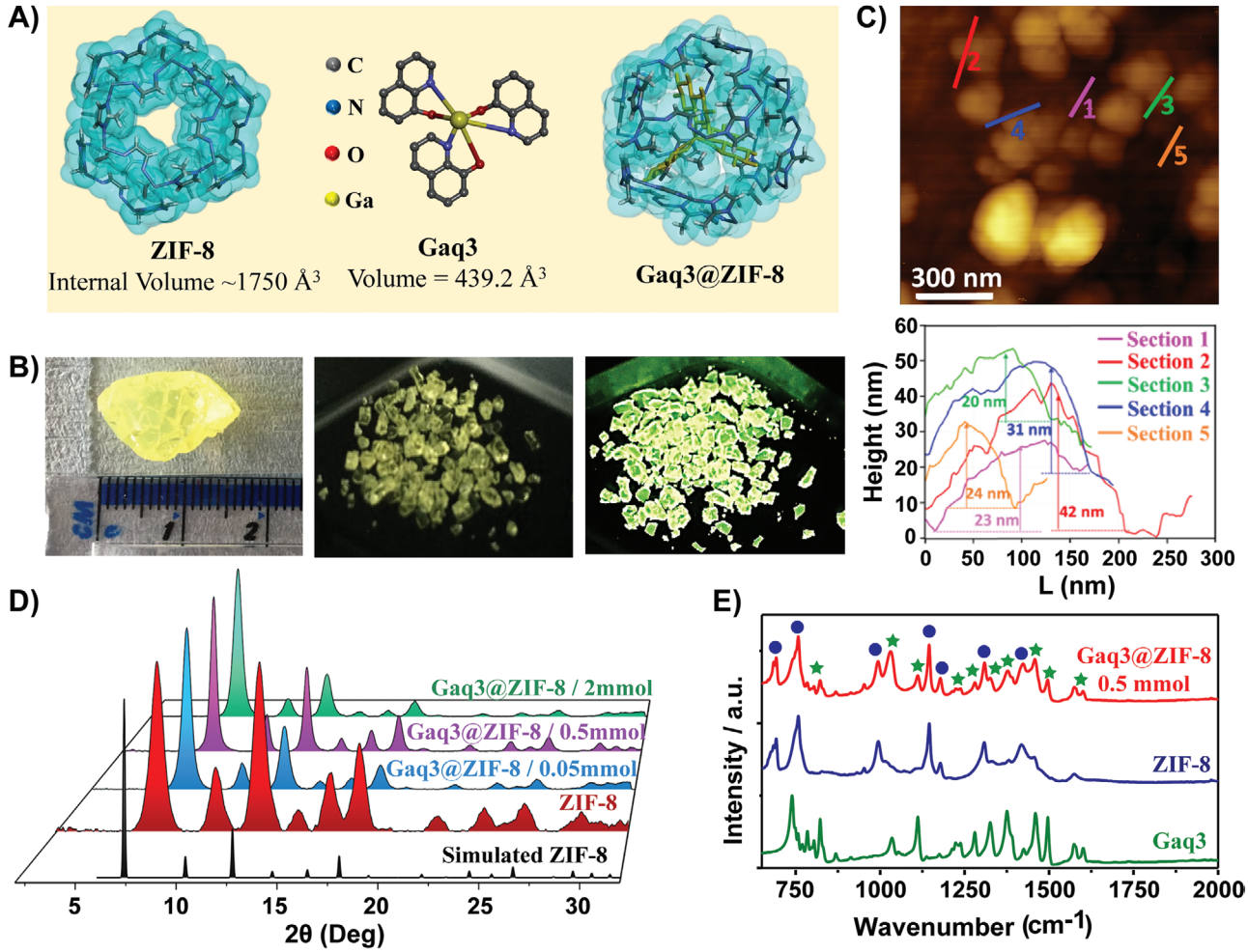

Figure 1. A) Representation of the chemical structures of ZIF-8 (host pore volume ≈1750 Å^3), Gaq3 (guest volume ≈440 Å^3), and the Guest@MOF composite Gaq3@ZIF-8. B) Photos of a big monolith (≈1.5 cm, left photo) and small monoliths of Gaq3@ZIF-8 (0.5 mmol) in daylight (middle photo) and under 365 nm UV (right photo), respectively. C) AFM topography image (top figure) of Gaq3@ZIF-8 (0.5 mmol) revealing the nanoscale morphology and the height profiles (bottom figure, height 20–40 nm) corresponding to the marked regions in the AFM image. D) PXRD patterns of the simulated ZIF-8, pristine ZIF-8, and the different Gaq3@ZIF-8 composites synthesized with 0.05, 0.5, and 2 mmol of Gaq3, respectively. E) FTIR spectra of Gaq3 (green), ZIF-8 (blue), and Gaq3@ZIF-8 (0.5 mmol) composites, which show a combination of the vibrational bands that are characteristic of Gaq3 guest (green stars) and ZIF-8 host (blue dots).

characteristics of the vibrational modes of the hydroxyquinoline ligands in Gaq3, specifically the bands at 1460 cm^{-1} (quinoline CC/CN stretching + CH bending) and at 1500 cm^{-1} (pyridyl and phenyl CC/CN stretching + CH bending vibration).[38,39] Similarly, the FTIR spectrum of Gaq3@ZIF-8 also displays characteristic bands of ZIF-8 as the band at 1584 cm^{-1} (C=N stretch mode) and the bands in the regions of 1350–1500 cm^{-1} (associated with the entire ring stretching) and 900–1350 cm^{-1} (in-plane bending of the mIm ring).[40] This combination of FTIR features unequivocally confirms the presence of Gaq3 present in the framework of the ZIF-8 host.

2.2. UV–Vis Reflectance, Emission, and Time-Resolved Luminescence Properties of Gaq3@ZIF-8

The solid-state diffuse reflectance spectra (converted to Kubelka–Munk, K–M function) of the different Gaq3@ZIF-8 (0.05, 0.5, and 2 mmol) composites also revealed the presence of Gaq3 in ZIF-8. As shown in **Figure 2**A, the K–M spectra of Gaq3@ZIF-8 exhibits the typical absorption bands of the Gaq3 metal complexes with maxima located at ≈266 and ≈390 nm, attributed to the electronic transitions between the bonding and anti-bonding molecular orbitals of the quinolate ligands such as $\sigma \rightarrow \sigma^*$ (266 nm) and $\pi \rightarrow \pi^*$ (390 nm).[39,41] It is worth noting that the K–M spectrum of pure Gaq3 in powder form is much broader and red-shifted compared to those observed for Gaq3@ZIF-8 composites, or when compared to the absorption spectra of pure Gaq3 dispersed in organic solvents (e.g., DMF or acetone, see Figure S2, Supporting Information), proving that Gaq3 complexes have been isolated by the pores of ZIF-8 as a result of nanoconfinement.

The excitation spectra of Gaq3@ZIF-8 (0.05, 0.5, and 2 mmol) composites depicted in Figure 2B are comparable to the K–M spectra, indicating a common origin of the excited states (photoexcited Gaq3 complexes) and the ground state.

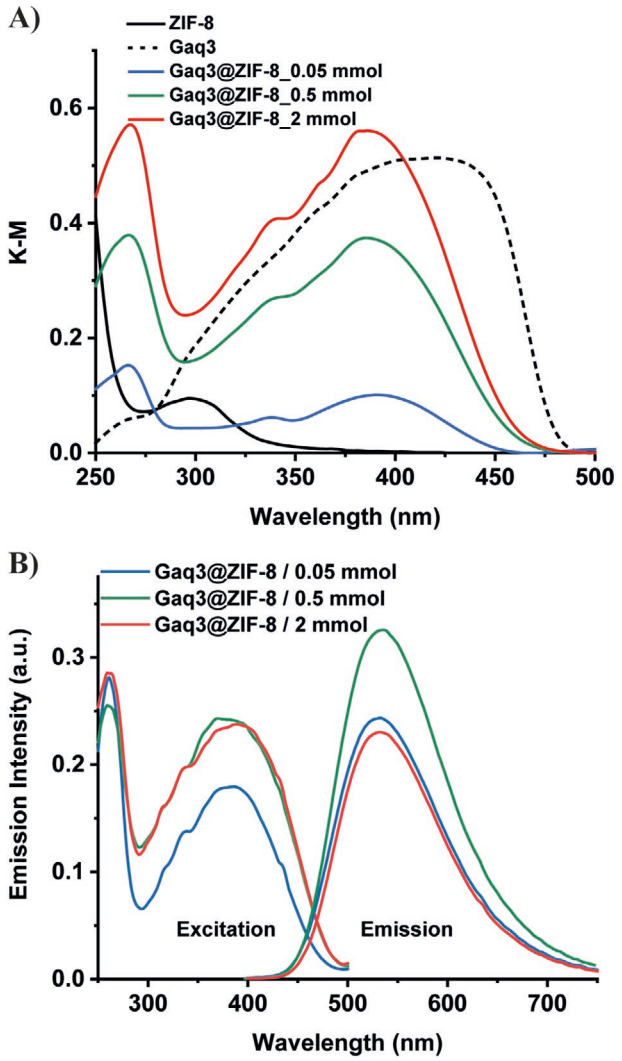

Figure 2. A) Diffuse reflectance spectra transformed to Kubelka–Munk (K–M) function for the powder samples of ZIF-8, Gaq3, and the different Gaq3@ZIF-8 (Guest@MOF) composites synthesized with 0.05, 0.5, and 2 mmol of Gaq3, respectively. B) Excitation and emission spectra of powder samples of Gaq3@ZIF-8 with 0.05, 0.5, and 2 mmol of Gaq3, respectively. For the emission spectra, the samples were excited at 390 nm, while the excitation spectra were recorded at 535 nm.

The emission spectra of all Gaq3@ZIF-8 composites are very similar in shape with a maximum at ≈535 nm and a full width at half maximum (FWHM) of ≈4160 cm^{-1}, in agreement with previous observations for Gaq3,[42,43] however Gaq3@ZIF-8 (0.5 mmol) exhibits higher emission intensity than the other two samples. The luminescence quantum yield ($QY_{(\lambda Exc = 390\ nm)}$) amounted to 15% for the Gaq3@ZIF-8 (0.05 and 0.5 mmol) and decreases to 8% for the Gaq3@ZIF-8 (2 mmol) composite. The decline observed in the QY value for the sample with the highest amount of Gaq3 could be attributed to the inner filter effect or to the aggregation of Gaq3 complexes. At first instance, the QY values of the 0.05 and 0.5 mmol Gaq3@ZIF-8 materials are the same, however the latter has a higher amount of Gaq3, and thus its emission will be higher (Figure 2B). The Gaq3@ZIF-8 (0.5 mmol) composite was therefore identified as the most suitable material for subsequent use in the fabrication of luminescent devices.

To gain further insights into the photoluminescence properties of Gaq3@ZIF-8 materials, the fluorescence decay was determined using time-correlated single-photon counting (TCSPC) technique and the obtained decays were compared to those of pure Gaq3 and pristine ZIF-8 in powder form (Figure S3, Supporting Information). All decays could be fitted to a sum of exponentials ($I(t) = \sum \alpha_i \exp^{-t/\tau_i}$). Upon excitation at 365 nm, the fluorescence decay of pure Gaq3 in the solid-state can be fitted to a bi-exponential decay with two time components of $\tau_1 \approx 6$ ns and $\tau_2 \approx 19$ ns (Table S1, Supporting Information) at several wavelengths between 475 nm and 650 nm. The determined values of the decay times agree with those obtained for other hydroxyquinolate metal complexes such as Alq3 and Znq2.[44,45] Likewise, the fluorescence decay of a sample of the pristine host, ZIF-8, which is upon excitation at 365 nm characterized by an emission spectrum with maximum around 440 nm (Figure S4, Supporting Information), can be fitted to a bi-exponential decay with decay times of $\tau_1 \approx 2$ ns and $\tau_2 \approx 11$ ns (Table S2, Supporting Information). The contribution of both decay times shows no significant wavelength dependence, thereby suggesting the presence of a single emitting species. However, the fluorescence decay of the Gaq3@ZIF-8 composites between 475 and 650 nm is more complex. While at 475 and 535 nm it has to be analyzed as a sum of three exponentials with decay times of $\tau_1 \approx 1$ ns, $\tau_2 \approx 9$ ns, and $\tau_3 \approx 24$ ns (Table S3, Supporting Information), at 650 nm it can be analyzed as a sum of two components with decay times of $\tau_2 \approx 9$ ns and $\tau_3 \approx 23$ ns. Comparing those decay times with the ones of Gaq3 and ZIF-8 suggests that the decay obtained for Gaq3@ZIF-8 could be a combination of the decays of Gaq3 and ZIF-8 at 475 and 535 nm while at 650 nm it is mainly due to Gaq3. This means that the shortest decay component which is only observed at 475 and 535 nm can be attributed to the emission of ZIF-8. Energy transfer from ZIF-8 to Gaq3 could explain why the ZIF-8 emission decays faster in Gaq3@ZIF-8 than in pristine ZIF-8. This possibility is further supported by the overlap existing between the emission spectrum of ZIF-8 and the absorption of Gaq3 (Figure S4, Supporting Information). The two other components with decay times of ≈9 and ≈23 ns must then be attributed to Gaq3 encapsulated into ZIF-8. It is quite unlikely that the component with the intermediate decay time of ≈9 ns contains an important contribution of ZIF-8 emission as its amplitude (a_2) and contribution (c_2) become larger at longer wavelengths. One should note that the decay times of the components with the intermediate and long decay time are somewhat larger than those found for pure Gaq3 ($\tau_2 \approx 9$ ns and $\tau_3 \approx 23$ ns vs $\tau_2 \approx 6$ ns and $\tau_3 \approx 19$ ns).

In agreement with our previous assumptions, the increase in the lifetime value of Gaq3@ZIF-8 is owing to a guest–host confinement effect of Gaq3 into the pores of ZIF-8, which increases the rigidity of the guest molecules, and thus increases their lifetime by decreasing the rate of internal conversion. It is important to remark that although the features of the fluorescence decays of Gaq3@ZIF-8 (0.05 and 0.5 mmol) are similar, the values of the τ_2 and τ_3 components (the ones involving Gaq3 contribution) are slightly reduced ($\tau_2 \approx 7$ ns and $\tau_3 \approx 19.5$ ns, see Table S3, Supporting Information) for Gaq3@ZIF-8 (2 mmol).

From this observation, we reasoned that the quenching of the luminescence of Gaq3@ZIF-8 (2 mmol) is more likely due to an aggregation of Gaq3 metal complexes,[46] however we cannot rule out the possibility of an inner filtering effect as previously reported for other MOF systems.[47]

2.3. Long-Term Material Stability

As the major aim of this work is to develop proof-of-concept solid-state lighting devices using Guest@MOF LMOFs, we selected Gaq3@ZIF-8 (0.5 mmol) to explore the long-term stability of the related materials, as it is the combination which exhibits the highest emission intensity as described above. The material robustness of Gaq3@ZIF-8 (0.5 mmol) has been investigated by means of PXRD and luminescence QY measurements of the sample right after its synthesis and then re-examined after a period of 8 months. As shown in Figure S5A (Supporting Information), there are no detectable changes in the position or in the intensity of the PXRD peaks of Gaq3@ZIF-8 after 8 months, indicating that the crystalline structure of ZIF-8 remains stable after this period. Although no changes in the crystalline structure were observed, it is very common that the luminescence properties of the MOF materials can be affected, or its structure being altered (amorphized for instance) after this relatively long period of time. Remarkably, we determined that the QY value (15%) of Gaq3@ZIF-8 after 8 months is exactly the same as when it was measured right after its synthesis (Figure S5B, Supporting Information), unequivocally demonstrating the success of our methodology by trapping Gaq3 into ZIF-8 pores which acts as a shield for protecting the encapsulated guests from photodegradation.

2.4. Down-Converter MOF-WLED Incorporating Gaq3@ZIF-8

By leveraging the high similitude between the emission of Gaq3@ZIF-8 (CIE coordinates: 0.33, 0.51) and the commercial Ce^{3+}:YAG (CIE coordinates: 0.42, 0.56), alongside the relatively high QY value of our material in the solid-state, we constructed a new down-converter type MOF-WLED by dipping a 405 nm LED into a homogenous dispersion of Gaq3@ZIF-8 in the transparent PMMA polymer (see Experimental Section for more information). As shown in **Figure 3**A, the combination of the 405 nm violet light of the LED and the green-yellowish emission of the coating due to the Gaq3@ZIF-8 layer produces a cool white light with a correlated color temperature (CCT) of ≈5600 K and with CIE coordinates of (0.27, 0.34), which are not far from the ideal ones at (0.33, 0.33). Notably, this simple methodology enables a uniform coating of the LED bulb, thereby generating to a very well distributed emission of white light as shown in Figure 3B.

2.5. Electroluminescent MOF-LED Incorporating Gaq3@ZIF-8

In the preceding section, we have shown the down-converter light emission device, however it is an increasingly common requirement for the industry to use the phosphors as an

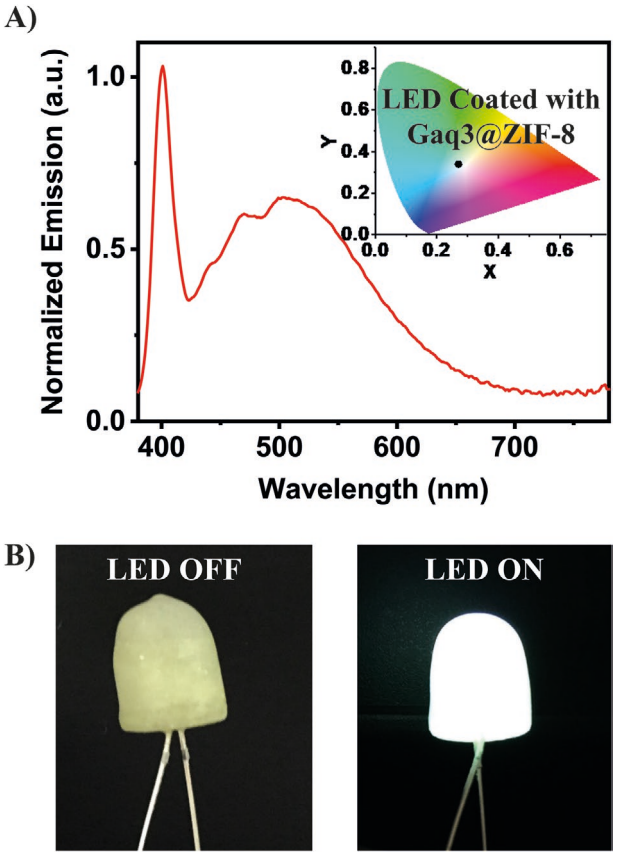

Figure 3. A) Emission spectrum of the 405 nm LED coated by Gaq3@ZIF-8 (0.5 mmol) dispersed in a PMMA polymer matrix. The inset is a representation of the CIE (1936) coordinates of the device (0.27, 0.34). B) Photo of the turn-off (left) and turn-on (right) down-converter MOF-LED device.

electroactive layer, due to the easier preparation and higher stability over time. On that basis, the following approach was moved toward the use of Gaq3@ZIF-8 as an electroactive material (EM) in the LED configuration. In the simplest case, for a single layer device, the Gaq3@ZIF-8 layer would be sandwiched between an indium-tin-oxide (ITO glass) electrode and a metal top electrode. Since the number of transport sites on the ZIF-8 MOF is much higher than that on Gaq3 in the Gaq3@ZIF-8 composite, the charge carriers will mainly move through the ZIF-8, and consequently the device design should mainly consider the conduction and valence bands of ZIF-8. The specific values reported for the CB and VB of ZIF-8 are at ≈0.9 and 6.4 eV,[48,49] at below the vacuum level respectively. Therefore, additional layers like PEDOT:PPS and p-PBD [2-(4-tert-butylphenyl)-5-(4-biphenylyl)-1,3,4-oxadiazole] should be included into the LED configuration as a hole injection and electron injection layers, respectively. The reason behind this insertion is to reduce the large mismatch between the ZIF-8 energy levels and the electrodes used (ITO glass and aluminum cathode) and at the same time to improve the balance of carrier injection rate in the device.[50]

Figure 4A depicts a schematic of the device architecture used: ITO anode/PEDOT:PSS (thickness 40 nm)/Gaq3@ZIF-8 (thickness 150 nm)/p-PBD (thickness 5 nm)/Al

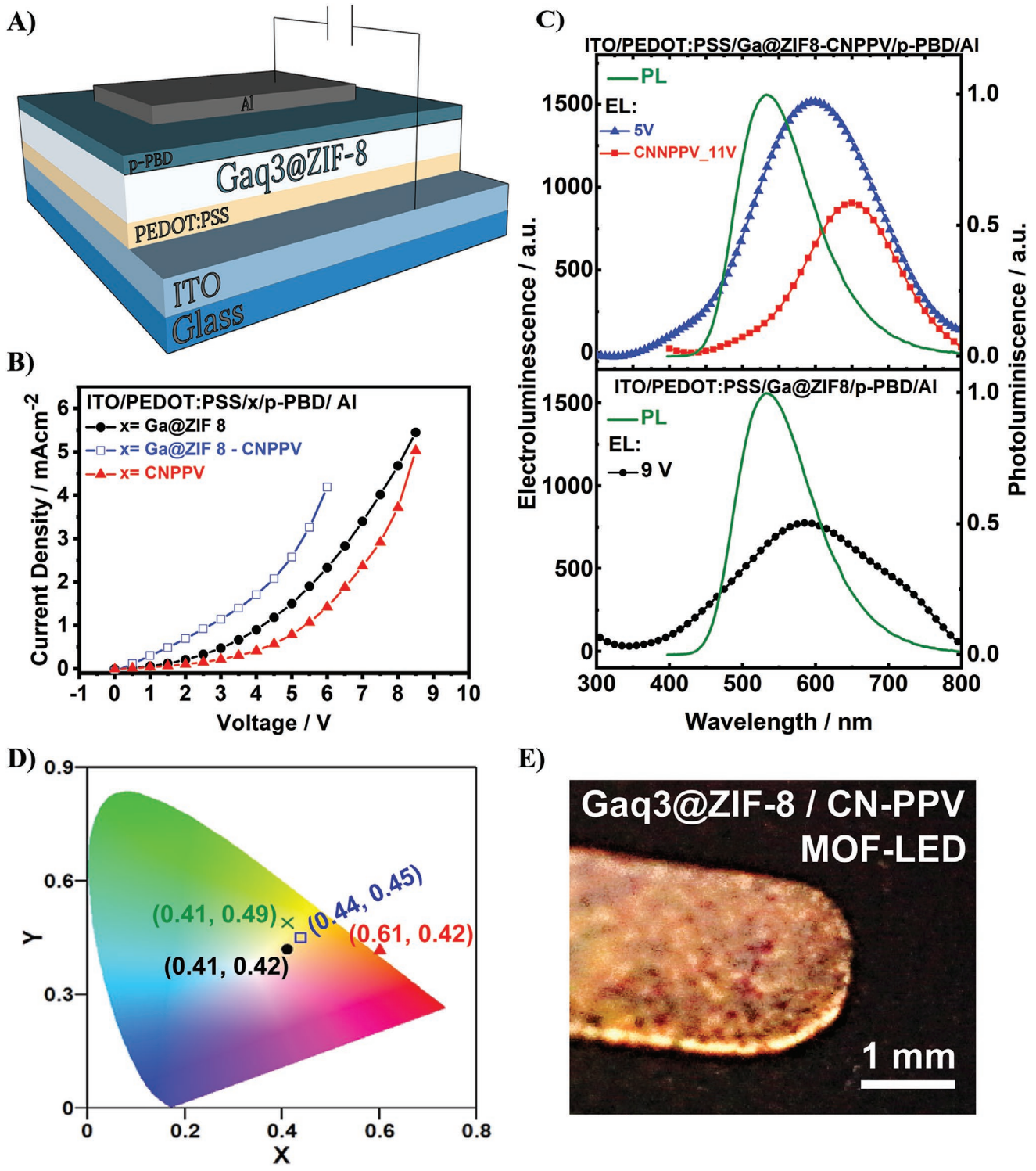

Figure 4. A) Schematic representation of the LED device architecture, where the Gaq3@ZIF 8 composite acts as the electroluminescent layer with a thickness of ≈150 nm. B) Comparison of the current versus voltage curves, and C) their corresponding electroluminescent spectra of the MOF-LED devices (Gaq3@ZIF-8/CNPPV–blue, and Gaq3@ZIF-8–black) and the device fabricated only with the CNPPV polymer (red). The green line is the photoluminescence spectrum of the powder form of Gaq3@ZIF-8. D) Graph displaying the CIE coordinates corresponding to the photoluminescence of Gaq3@ZIF-8 (green cross) and the electroluminescence of the different MOF-LEDs (Gaq3@ZIF-8/CNPPV: blue square, and Gaq3@ZIF-8: black dot) and CNPPV-LED (red triangle). E) Photo of the turn-on Gaq3@ZIF-8 / CNPPV MOF-LED device operating at 6 V, showing the characteristic orange-yellowish emission.

cathode (thickness 150 nm). The values of the thickness were extracted from profilometer traces and an example of which is shown in Figure S6A (Supporting Information). It is worth noting that the data from this proof-of concept unsealed device was recorded outside the glovebox, which reflects the high stability of the working device under ambient conditions. The current–voltage (*I*–*V*) curve of the device (Figure 4B) shows the typical diode characteristics with a turn-on voltage of 3 V.[51] To obtain further insights on the OLED optoelectronic properties, the electroluminescence (EL) spectrum at 9 V was recorded (Figure 4C). The EL spectra show a broad spectrum spanning from 400 to 800 nm (FWHM of 7285 cm^{-1}) with its maximum intensity at 585 nm. The recorded EL spectrum is red-shifted and broader than the photoluminescent (PL) one, suggesting that excited state species differing from excited Gaq3 molecules are generated under forward voltage. To shed light into the origin of the EL mechanism, a Gaussian spectral deconvolution of the EL was performed (Figure S6B, Supporting Information). Two bands centered at 534 and 648 nm with a relative contribution of 35% and 65%, respectively (from the total intensity) were observed. It is worth noting that the 534 nm component is exactly matching the PL spectrum underlining the same origin of the emission. On the other hand, the origin for the 648 nm contribution, not present in the PL spectrum, could be explained by the presence of different types of defects as it has previously been reported for similar inorganic and hybrid systems.[13,14,28] The most plausible mechanism for this new component is the electron-hole recombination at the grain boundaries due to the formation of EM layer by MOF crystals (≈200 nm). In order to reduce the number of those traps and with the aim of increasing the homogeneity of the EM layer, the Gaq3@ZIF-8 was dispersed into host polymeric matrices. As a first attempt, a nonconductive polystyrene film was used as a host matrix as it does not modify the optoelectronic properties of the EM layer. For this sample we obtained only very small currents and no emission from the LED. This indicates that a thin nonconducting polystyrene layer envelops the crystals and inhibits intercrystal transport of charge carriers. Therefore we replaced polystyrene by polyvinylcarbazole (PVK) which has reasonably good hole transport properties and some electron transport properties.[13,14,28] In this case, higher currents were obtained, but still no stable EL was observed. This information highlights that the presence of PVK enhances the charge mobility, mainly due to a higher hole mobility, however as there was no (or a very poor) balance between the electron and hole injection rate and/or mobility, no electroluminescence was observed.

To solve this problem, the CN-PPV polymer [poly(5-(3,7-dimethyloctyloxy-2-methoxy-cyanoterephthalydiene] which also behaves as an electron transport material was used to disperse the Gaq3@ZIF-8 in the EM layer. A film of 190 nm thickness was obtained (Figure S6A, Supporting Information) and a photo of the orange-yellowish emission working device at 6 V is shown in Figure 4E. As in the case mentioned above, the devices were tested in ambient conditions without any sealing. Interestingly, in this case, the turn-on voltage of this device configuration is reduced by 1.5 V compared to the device without any polymer (from 3 to 1.5 V) meanwhile the current density at 6 V is enhanced by approximately twofold (from ≈2 to ≈4.5 mA cm^{-2}). Surprisingly, the EL intensity was enhanced by twofold even when using about half of the voltage (5 V instead of 9 V) in comparison with the device without a polymer matrix. Furthermore, no differences in spectral position and FWHM were observed (Figure 4). These results suggest that the role of the polymer is only to improve the balanced injection or/and mobility of the charges without modifying the EL emission. To confirm this assumption and for discarding the contribution of EL emission from the polymer, a pristine CN-PPV LED (without the MOF) using the same device configuration was fabricated. Figure 4B,C display the *I*–*V* curves and the EL spectra, where higher turn-on voltage (4 V) and weaker EL at 11 V forward voltage were obtained when compared to the parent device with Gaq3@ZIF-8. These observations along with the results obtained from the Gaussian deconvolution of the emission spectrum of the Gaq3@ZIF-8 / CN-PPV LED (Figure S6B, Supporting Information), where exactly the same two emissive species and contributions were obtained as in the Gaq3@ZIF-8 devices without CN-PPV, have enabled us to establish two important findings: i) the contribution of the polymer toward the EL behavior is small as its 661 nm band slightly contributes to the total signal in the Gaq3@ZIF-8/CN-PPV device, and ii) the 648 nm band, only observed in the device with Gaq3@ZIF-8 (without CN-PPV), might be related to defects present in the MOF framework. The warrants further study to confirm the role of defects in the context of EL emission.

It has been reported that ZIF-8 could develop point defects by its interaction with the environment.[52] The most plausible type of defect will be a linker vacancy due to the presence of atmospheric moisture. Similar to the oxygen vacancies in zeolites, this defect originates from protonation of the linker which breaks the linker-Zn bond and hence the Zn cluster will become coordinated with the water to form Zn-OH···H_2O-Zn.[52] Once the defect is formed, the spontaneous formation of more defects is enhanced because the formation energy of the second or third defect is further reduced.[53] We reasoned that the presence of this type of defects could act as a trap for charge carriers, where the electron-hole recombination happens. Interestingly, the spectral position at ≈650 nm is reminiscent of the EL observed for the oxygen vacancies present in ZnO materials (620–690 nm).[54,55] From this observation it can be drawn that the reddest component (650 nm) is obtained when the electron-hole recombination occurs in the oxygen vacancies associated with the missing linker defects.

Finally, Figure S6C (Supporting Information) summarizes the enhancement of the optoelectronic properties of the proof-of-principle study of Gaq3@ZIF-8 versus Gaq3@ZIF-8/CN-PPV LED. The CIE coordinates depicted in Figure 4D demonstrate the small differences in the values obtained between them and against the ideal cool white light located at (0.33, 0.33). The results show the potential applicability of Gaq3@ZIF-8 emissive layer as a new electroluminescent material. Therefore, by unravelling the EL mechanism behind these proof-of-concept devices, we lay the groundwork for future MOF-based LEDs, where it was shown that a more controlled deposition technique is required to reduce non-desired electron-hole recombination.

3. Conclusions

In this study we have developed a series of novel LMOF composites based on the Guest@MOF principle, where the well-known semiconducting metal-complex, Gaq3, was straightforwardly encapsulated into the nanopores of the zeolitic MOF structure called ZIF-8. The structural, physicochemical and photoluminescent properties of these composites were explored, clearly demonstrating that the crystalline structure of the ZIF-8 host remains stable upon the nanoconfinement of Gaq3 guests, and that the luminescent properties of the composite materials originated mainly from the Gaq3 dye, even though some contribution of ZIF-8 emission was also detected through the emission lifetime components. The excellent physical (long-term reliability and robustness) and luminescent (relatively high and reliable QY value in solid-state) properties of Gaq3@ZIF-8 materials, stimulated us to fabricate two examples of MOF-LED devices. In the first case, a 405 nm LED was coated with Gaq3@ZIF-8 nanoparticles dispersed in PMMA polymer. The combination of blue and yellow emissions of the LED and Gaq3@ZIF-8, respectively, have allowed the fabrication of a down-converter MOF-WLED that exhibits a uniform white light emission. In the second example, the Gaq3@ZIF-8 composite was used as the electroluminescent material in a multilayer proof-of-concept EL device. It was demonstrated that the device containing only Gaq3@ZIF-8 exhibited an *I–V* curve characteristics of LEDs with a turn-on voltage of 3 V, as well as a broadband electroluminescence spectrum. Remarkably, by dispersing the Gaq3@ZIF-8 in CN-PPV polymer, the turn-on voltage was reduced to 1.5 V and the electroluminescence efficiency was improved by about twofold. Additionally, the mechanism of the electroluminescence was also discussed, and concluded that the broadband electroluminescence has originated from a combination of electron-hole recombination in both the Gaq3 dye and the oxygen vacancies present in the ZIF-8 framework. The results presented here elucidate the enormous potential of LMOFs to enable fabrication of new LED technologies, opening the door for future developments in the almost unexplored field of electroluminescent MOF-LEDs.

4. Experimental Section

Materials: Zinc nitrate hexahydrate ($Zn(NO_3)_2{\cdot}6H_2O$), 2-methylimidazole (mIm), gallium (III) nitrate hydrate ($Ga(NO_3)_3{\cdot}H_2O$), 8-hydroxyquinoline (8-HQ), triethylamine (NEt_3), poly(methyl methacrylate) (PMMA), methanol (MeOH), and dichloromethane (DCM) were purchased from Fisher Scientific and used without further purification.

Synthesis of Gaq3, ZIF-8, and Gaq3@ZIF-8—Synthesis of Gaq3: Gaq3 metal complex was synthesized following a previously reported protocol with some modifications.[56] Briefly, 2 mmol of $Ga(NO_3)_3{\cdot}H_2O$ and 6 mmol of 8-HQ were dissolved in 20 mL of MeOH. The mixture was stirred for 3 h and the yellow solid sample was washed with copious amount of MeOH, collected by centrifugation (8000 rpm, 10 min) and dried at 100 °C for 3 h.

Synthesis of Gaq3, ZIF-8, and Gaq3@ZIF-8—Synthesis of ZIF-8: ZIF-8 was synthesized following the previously described high concentration reaction (HCR) methodology with some modifications.[57] Briefly, 4 mmol of $Zn(NO_3)_2{\cdot}6H_2O$ were dissolved in 10 mL of MeOH. Another solution was prepared by mixing 16 mmol of mIm and 16 mmol of NEt_3 in 10 mL of MeOH. Then, both solutions were combined and a white gel was promptly formed. The mixture was sonicated for 10 min, washed with copious amount of MeOH, collected by centrifugation (8000 rpm, 10 min) and dried at 100 °C for 3 h. The addition of NEt_3 is needed to deprotonate the mIm linker, which will cause not only an acceleration of the reaction, but also an increase in the amount of obtained material and the downsizing of the 3D framework of ZIF-8 to yield nanocrystals.

Synthesis of Gaq3, ZIF-8, and Gaq3@ZIF-8—Synthesis of Gaq3@ZIF-8 Composites: Three different Gaq3@ZIF-8 composites with different amounts of Gaq3 (0.05, 0.5, and 2 mmol) have been synthesized following a similar procedure to the one described above. Essentially, 4 different solutions were prepared by dissolving the following reagents in 10 mL of MeOH each: A) 4 mmol of $Zn(NO_3)_2{\cdot}6H_2O$, B) 16 mmol of mIm and 16 mmol of NEt_3, C) 0.05, 0.5, and 2 mmol of $Ga(NO_3)_3{\cdot}H_2O$, and D) 0.15, 1.5, and 6 mmol of 8-HQ. While the amounts of $Zn(NO_3)_2{\cdot}6H_2O$, mIm and NEt_3 remain constant, the amounts of $Ga(NO_3)_3{\cdot}H_2O$ and 8-HQ were increased from 0.05 → 0.5 → 2 and 0.15 → 1.5 → 6 mmol, respectively, resulting in 3 different composites with different amounts of Gaq3, which were designated as Gaq3@ZIF-8 (0.05 mmol), Gaq3@ZIF-8 (0.5 mmol) and Gaq3@ZIF-8 (2 mmol), respectively. Once the above solutions were prepared, (C) and (D) were first mixed and stirred for 1 min until a clear yellow solution was observed. After that, solutions (B) and (A) were consecutively added to the latter mixture and a prompt formation of pale-yellow gels was observed. The gels were sonicated for 10 min, washed with copious amount of MeOH, collected by centrifugation (8000 rpm, 10 min) and dried at 100 °C for 3 h. It is important to mention that the samples were washed until a transparent and nonemissive supernatant was obtained in order to remove all excess Gaq3 complexes deposited on the ZIF-8 surface. It's demonstrated that if the composite samples are not thoroughly washed, the emission of the Gaq3@ZIF-8 composite resembles the emission of Gaq3 in the powder form, clearly indicating that the emission originated mainly from the agglomeration of Gaq3 metal complexes adhered to the surface of ZIF-8 (Figure S1, Supporting Information).

Materials Characterization: The crystalline structure, chemical and luminescent properties of pure Gaq3, pristine ZIF-8, and Gaq3@ZIF-8 guest@MOF composites were investigated by a combination of X-ray, spectroscopy, and microscopy techniques. Powder X-ray diffraction experiments were carried out in a Rigaku MiniFlex X-ray diffractometer with a Cu Kα source (1.541 Å). The diffraction data were collected using 0.01° step size, 1° min^{-1} scan rate and at 2θ angle ranging from 2° to 32°. Atomic force microscopy micrographs were collected using a Veeco Dimension 3100 microscope. Fourier-transform infrared spectra were recorded on a Nicolet iS10 FTIR spectrometer. The FTIR spectrum of each sample was collected 3 times and then averaged. Steady-state UV–vis diffuse reflectance spectra were collected in a UV-2600 (Shimadzu) spectrophotometer and the raw data transformed using the Kubelka–Munk function. Steady-state fluorescence spectra, luminescence quantum yields and time-resolved emission decays were recorded using the FS-5 spectrofluorometer (Edinburgh Instruments) equipped with different modules for each specific experiment (i.e., integrating sphere for quantum yield and a standard solid sample holder for powder experiments). For time-resolved measurements, the samples were pumped with a 365 nm EPLED picosecond pulsed laser source. The instrument response function (IRF, ≈800 ps) was used to deconvolute the emission decays. The decays were fitted to a multiexponential function and the quality of the fit was estimated by the value of χ^2, which was always below 1.3.

Down-Converter MOF-WLED Fabrication: The down-converter MOF-WLED was easily fabricated by dipping a 405 nm LED bulb into a mixture of Gaq3@ZIF-8 (0.5 mmol) and PMMA polymer in DCM. That mixture was prepared by sonicating 50 mg of Gaq3@ZIF-8 (0.5 mmol) in 2 mL of DCM for 30 min until a homogeneous suspension was obtained. Then, 1 mL of a 10% w/w solution of PMMA in DCM was added to the latter suspension and the mixture was sonicated for another 30 min. After that, the 405 nm LED bulb was dipped and dried several times (typically between 5–10 times) until a homogeneous coating was obtained. The emission spectrum of the down-converter LED was recorded using the UPRtek MK350N Plus spectrophotometer.

Electroluminescent MOF-LED Fabrication: For the fabrication of the LED using Gaq3@ZIF-8 (0.5 mmol) as the electroluminescent layer

a methodology described elsewhere is followed.[28] Briefly, indium-tin-oxide (ITO) coated glass substrates with a sheet resistance of ≈10^9 Ω cm were first cleaned in an ultrasonic bath using the alkaline detergent (Hellmanex solution) for 10 min, followed by their successive sonication for 10 min in water, acetone, and isopropanol. To remove any contamination on the ITO-coated glass, it was exposed to ozone for 30 min, which at the same time help to reduce the work function of the ITO.[58] After that, around 1 mL of PEDOT:PSS (Sigma-Aldrich, high conductivity) solution, which acts as the hole injection layer, was spin coated at 3000 rpm for 90 s and subsequently annealed at 140 °C for 10 min. Then, a suspension of Gaq3@ZIF-8 (0.5 mmol) in chlorobenzene (10 mg mL^{-1}) or a dispersion of 10 mg of Gaq3@ZIF-8 in a 2.5 mg mL^{-1} solution of poly(5-(3,7-dimethyloctyloxy-2-methoxy-cyanoterephthalydiene) (CN-PPV) in chlorobenzene (Sigma-Aldrich, anhydrous) were sonicated for 1 h, spin coated at 1000 rpm for 60 s and annealed for 10 min at 80 °C. Afterward, a 5 mg mL^{-1} solution of the electron injection layer, 2-(4-*tert*-butylphenyl)-5-(4-biphenylyl)-1,3,4-oxadiazole (PBD, Sigma Aldrich) in cyclohexane, was spin coated at 6000 rpm for 90 s and the layer was annealed at 80 °C for another 10 min. Finally, a 150 nm thick layer of the aluminum electrode was vapor deposited on the top of the latter layer.

Supporting Information

Supporting Information is available from the Wiley Online Library or from the author.

Acknowledgements

This work was supported by the ERC Consolidator Grant through the grant agreement 771575 (PROMOFS) and the EPSRC Impact Acceleration Account Award (EP/R511742/1). The authors thank the Research Complex at Harwell (RCaH) for access to the Nicolet iS10 FTIR and the Shimadzu UV-2600 spectrometers. This work was also supported by the Research Foundation-Flanders (FWO, Grant Nos. G.0B39.15 and G098319N), FWO postdoctoral fellowships to C.M. (Grant Nos. 12J1719N and 12J1716N), the KU Leuven Research Fund (C14/15/053), the Flemish government through long-term structural funding Methusalem (CASAS2, Meth/15/04), the Hercules Foundation (HER/11/14), and the Belgian Federal Science Policy Office (IAP-VII/05).

Conflict of Interest

The authors declare no conflict of interest.

Keywords

defects, electroluminescence, guest@MOF, luminescent MOF, MOF-LED, nanoparticles, thin film devices

Received: April 19, 2020
Revised: May 24, 2020
Published online: June 11, 2020

[1] U. S. D. Energy How Energy-Efficient Light Bulbs Compare with Traditional Incandescents, https://www.energy.gov/energysaver/save-electricity-and-fuel/lighting-choices-save-you-money/how-energy-efficient-light (accessed: October 2019).
[2] Y.-C. Li, Y.-H. Chang, P. Singh, L.-B. Chang, D.-H. Yeh, T.-Y. Chao, S.-Y. Jian, Y.-C. Li, C. M. Tan, C.-S. Lai, L. Chow, S.-P. Ying, *Materials* **2018**, *11*, 365.
[3] Q. Song, X. Xu, J. Liu, X. Bu, D. Li, P. Liu, Y. Wang, J. Xu, K. Lebbou, *CrystEngComm* **2019**, *21*, 4545.
[4] M. Zhao, H. Liao, M. S. Molokeev, Y. Zhou, Q. Zhang, Q. Liu, Z. Xia, *Light: Sci. Appl.* **2019**, *8*, 38.
[5] J. Xing, F. Yan, Y. Zhao, S. Chen, H. Yu, Q. Zhang, R. Zeng, H. V. Demir, X. Sun, A. Huan, Q. Xiong, *ACS Nano* **2016**, *10*, 6623.
[6] Y. Ling, Z. Yuan, Y. Tian, X. Wang, J. C. Wang, Y. Xin, K. Hanson, B. Ma, H. Gao, *Adv. Mater.* **2016**, *28*, 305.
[7] M. K. Choi, J. Yang, T. Hyeon, D.-H. Kim, *npj Flexible Electron.* **2018**, *2*, 10.
[8] S. Jhulki, M. W. Cooper, S. Barlow, S. R. Marder, *Mater. Chem. Front.* **2019**, *3*, 1699.
[9] E. Coutiño-Gonzalez, W. Baekelant, J. A. Steele, C. W. Kim, M. B. J. Roeffaers, J. Hofkens, *Acc. Chem. Res.* **2017**, *50*, 2353.
[10] W. Baekelant, E. Coutino-Gonzalez, J. A. Steele, M. B. J. Roeffaers, J. Hofkens, *ACS Energy Lett.* **2017**, *2*, 2491.
[11] O. Fenwick, E. Coutiño-Gonzalez, D. Grandjean, W. Baekelant, F. Richard, S. Bonacchi, D. De Vos, P. Lievens, M. Roeffaers, J. Hofkens, P. Samorì, *Nat. Mater.* **2016**, *15*, 1017.
[12] D. Grandjean, E. Coutiño-Gonzalez, N. T. Cuong, E. Fron, W. Baekelant, S. Aghakhani, P. Schlexer, F. D'Acapito, D. Banerjee, M. B. J. Roeffaers, M. T. Nguyen, J. Hofkens, P. Lievens, *Science* **2018**, *361*, 686.
[13] K. Kennes, E. Coutino-Gonzalez, C. Martin, W. Baekelant, M. B. J. Roeffaers, M. Van der Auweraer, *Adv. Funct. Mater.* **2017**, *27*, 1606411.
[14] K. Kennes, C. Martin, W. Baekelant, E. Coutino-Gonzalez, E. Fron, M. B. J. Roeffaers, J. Hofkens, M. Van der Auweraer, *ACS Appl. Mater. Interfaces* **2019**, *11*, 12179.
[15] M. D. Allendorf, M. E. Foster, F. Léonard, V. Stavila, P. L. Feng, F. P. Doty, K. Leong, E. Y. Ma, S. R. Johnston, A. A. Talin, *J. Phys. Chem. Lett.* **2015**, *6*, 1182.
[16] W. P. Lustig, S. Mukherjee, N. D. Rudd, A. V. Desai, J. Li, S. K. Ghosh, *Chem. Soc. Rev.* **2017**, *46*, 3242.
[17] Y. Cui, J. Zhang, H. He, G. Qian, *Chem. Soc. Rev.* **2018**, *47*, 5740.
[18] H. Kaur, S. Sundriyal, V. Pachauri, S. Ingebrandt, K.-H. Kim, A. L. Sharma, A. Deep, *Coord. Chem. Rev.* **2019**, *401*, 213077.
[19] Q. Gong, Z. Hu, B. J. Deibert, T. J. Emge, S. J. Teat, D. Banerjee, B. Mussman, N. D. Rudd, J. Li, *J. Am. Chem. Soc.* **2014**, *136*, 16724.
[20] Z. Hu, G. Huang, W. P. Lustig, F. Wang, H. Wang, S. J. Teat, D. Banerjee, D. Zhang, J. Li, *Chem. Commun.* **2015**, *51*, 3045.
[21] Y. Lu, B. Yan, *Chem. Commun.* **2014**, *50*, 15443.
[22] A. Wang, Y.-L. Hou, F. Kang, F. Lyu, Y. Xiong, W.-C. Chen, C.-S. Lee, Z. Xu, A. L. Rogach, J. Lu, Y. Y. Li, *J. Mater. Chem. C* **2019**, *7*, 2207.
[23] C.-Y. Sun, X.-L. Wang, X. Zhang, C. Qin, P. Li, Z.-M. Su, D.-X. Zhu, G.-G. Shan, K.-Z. Shao, H. Wu, J. Li, *Nat. Commun.* **2013**, *4*, 2717.
[24] Y. Wen, T. Sheng, X. Zhu, C. Zhuo, S. Su, H. Li, S. Hu, Q.-L. Zhu, X. Wu, *Adv. Mater.* **2017**, *29*, 1700778.
[25] Z. Wang, C.-Y. Zhu, J.-T. Mo, P.-Y. Fu, Y.-W. Zhao, S.-Y. Yin, J.-J. Jiang, M. Pan, C.-Y. Su, *Angew. Chem. Int. Ed.* **2019**, *58*, 9752.
[26] D. Chen, H. Xing, Z. Su, C. Wang, *Chem. Commun.* **2016**, *52*, 2019.
[27] G. Haider, M. Usman, T.-P. Chen, P. Perumal, K.-L. Lu, Y.-F. Chen, *ACS Nano* **2016**, *10*, 8366.
[28] M. Gutiérrez, C. Martin, K. Kennes, J. Hofkens, M. Van der Auweraer, F. Sánchez, A. Douhal, *Adv. Opt. Mater.* **2018**, *6*, 1701060.
[29] A. K. Chaudhari, I. Han, J.-C. Tan, *Adv. Mater.* **2015**, *27*, 4438.
[30] A. K. Chaudhari, H. J. Kim, I. Han, J.-C. Tan, *Adv. Mater.* **2017**, *29*, 1701463.
[31] P. E. Burrows, L. S. Sapochak, D. M. McCarty, S. R. Forrest, M. E. Thompson, *Appl. Phys. Lett.* **1994**, *64*, 2718.
[32] F. Zhang, X. Liu, F. Huang, Z. Zhuo, L. Lu, Z. Xu, Y. Wang, X. Tao, W. Bian, W. J. C. S. B. Tang, *Chin. Sci. Bull.* **2011**, *56*, 479.
[33] A. Üngördü, *Chem. Phys. Lett.* **2019**, *733*, 136696.
[34] S. Agarwal, M. S. Haseman, A. Khamehchi, P. Saadatkia, D. J. Winarski, F. A. Selim, *Opt. Mater. Express* **2017**, *7*, 1055.

[35] Z. Shahedi, M. R. Jafari, *Appl. Phys. A* **2017**, *123*, 98.
[36] D. S. Biovia, *San Diego: Dassault Systèmes* **2016**, *2017*.
[37] C. F. Holder, R. E. Schaak, *ACS Nano* **2019**, *13*, 7359.
[38] Y.-W. Yu, C.-P. Cho, T.-P. Perng, *Nanoscale Res. Lett.* **2009**, *4*, 820.
[39] F. F. Muhammad, A Hapip, A. I.K. Sulaiman, *J. Organomet. Chem.* **2010**, *695*, 2526.
[40] Y. Hu, H. Kazemian, S. Rohani, Y. Huang, Y. Song, *Chem. Commun.* **2011**, *47*, 12694.
[41] L. G. Zhang, X. G. Ren, D. P. Jiang, A. D. Lu, J. S. Yuan, *Spectrosc. Lett.* **1996**, *29*, 995.
[42] W. Humbs, E. van Veldhoven, H. Zhang, M. Glasbeek, *Chem. Phys. Lett.* **1999**, *304*, 10.
[43] M. Brinkmann, B. Fite, S. Pratontep, C. Chaumont, *Chem. Mater.* **2004**, *16*, 4627.
[44] V. V. N. Ravi Kishore, K. L. Narasimhan, N. Periasamy, *Phys. Chem. Chem. Phys.* **2003**, *5*, 1386.
[45] T. Tsuboi, Y. Nakai, Y. J. C. E. J. o. P. Torii, *Cent. Eur. J. Phys.* **2012**, *10*, 524.
[46] S. Dhami, A. J. D. Mello, G. Rumbles, S. M. Bishop, D. Phillips, A. Beeby, *Photochem. Photobiol.* **1995**, *61*, 341.
[47] W. J. Newsome, S. Ayad, J. Cordova, E. W. Reinheimer, A. D. Campiglia, J. K. Harper, K. Hanson, F. J. Uribe-Romo, *J. Am. Chem. Soc.* **2019**, *141*, 11298.
[48] K. T. Butler, C. H. Hendon, A. Walsh, *J. Am. Chem. Soc.* **2014**, *136*, 2703.
[49] K. T. Butler, C. H. Hendon, A. Walsh, *Faraday Discuss.* **2017**, *201*, 207.
[50] Y. Shirota, H. Kageyama, *Chem. Rev.* **2007**, *107*, 953.
[51] C. Sah, R. N. Noyce, W. Shockley, *Proc. IRE* **1957**, *45*, 1228.
[52] C. Zhang, C. Han, D. S. Sholl, J. R. Schmidt, *J. Phys. Chem. Lett.* **2016**, *7*, 459.
[53] R. Han, N. Tymińska, J. R. Schmidt, D. S. Sholl, *J. Phys. Chem. C* **2019**, *123*, 6655.
[54] Ü. Özgür, A. livov, Y. I.C. Liu, A. Teke, M. A. Reshchikov, S. Doğan, V. Avrutin, S.-J. Cho, H. Morkoç, *J. Appl. Phys.* **2005**, *98*, 041301.
[55] N. H. Alvi, K. ulHasan, O. Nur, M. Willander, *Nanoscale Res. Lett.* **2011**, *6*, 130.
[56] J. C. S. Costa, C. F. R. A. C. Lima, L. M. N. B. F. Santos, *J. Phys. Chem. C* **2014**, *118*, 21762.
[57] A. K. Chaudhari, J.-C. Tan, *Nanoscale* **2018**, *10*, 3953.
[58] M.-F. Lo, T.-W. Ng, H.-W. Mo, C.-S. Lee, *Adv. Funct. Mater.* **2013**, *23*, 1718.